RSC Advances

PAPER

View Article Online
View Journal | View Issue

Cite this: *RSC Adv.*, 2025, **15**, 5751

Design of PVT driven forward osmosis and membrane distillation pilot plant for co-production of water and electricity

Ali Seid Ali *[ab] and Tijani Bounahmidi [a]

Desalination by photovoltaic thermal (PVT)-driven forward osmosis (FO) and membrane distillation (MD) stands out for its lower operational costs and reduced carbon emissions. However, the feasibility of a pilot-scale PVT-driven FO–MD system remains unexplored, which is crucial for industrialization. This study introduces a pilot PVT-FO–MD desalination system designed for simultaneous water and electricity production. The system aims to assess the feasibility of the process, evaluate its costs, and explore its potential for industrial applications. While PVT collectors have higher costs than standard PV panels, they offer improved electrical efficiency and additional thermal power generation, making them more efficient overall. The optimal design was tested using saline water with a concentration of 10 000 mg per liter and a NaCl draw solute with a concentration of 1 molarity. The system produces 172.1 kW h of thermal energy, 93.9 kW h of electrical energy, and 269 L of water daily. The FO water flux varies between 8.13 and 8.29 LMH, while the MD water flux fluctuates between 2.72 and 4.25 LMH throughout the year. Using average yearly weather data, the system produces 33 872 kW h of electrical energy, 65 846 kW h of thermal energy, and 106.84 m^3 of water annually. Increasing the desalination unit size boosts average water production to 126.47 m^3 annually. The project requires an initial capital investment of 212 741.38 USD. The return on investment is 11.84%, with a breakeven point at nine years. The net present value turns positive just before the end of the project's lifetime at a 10% interest rate. Although this type of system has not yet been commercialized, further studies are recommended to enhance its market competitiveness.

Received 21st October 2024
Accepted 14th February 2025

DOI: 10.1039/d4ra07525k

rsc.li/rsc-advances

1. Introduction

The rapid increase in the world population makes water supply more challenging.[1] Reports indicate that approximately 1.8 billion people face severe water scarcity, and water demand continues to grow.[2] Additionally, a recent study reported that one-third of the world's population lives under water-scarce situations.[3] Desalination is considered a reliable option for fresh water supply due to the abundance of seawater.[4] The desalinated water supply will reach 192 × 10^6 m^3 day^{-1} by 2050.[5] However, desalination consumes substantial energy. The growing demand for water in agriculture, industry, and drinking necessitates sustainable and cost-effective desalination methods. Since most desalination plants rely on fossil fuels, the associated carbon emissions encourage a shift towards renewable energy-driven desalination.[5]

Desalination powered by renewable energy offers advantages such as wide availability and low greenhouse gas emissions. Alawad *et al.* reviewed the integration of renewable energy with various desalination techniques and reported the following findings:[6] the use of geothermal energy in desalination process ensures continuous operation. Wind and solar energy powering reverse osmosis plants offer low-cost solution and represent mature technologies. Similarly, photovoltaic systems powering electrodialysis desalination are cost-competitive with fuel-driven electrodialysis systems. A recent study integrating photovoltaic systems with ultrafiltration and reverse osmosis reported benefits in clean water production and an enhanced energy-water nexus.[7]

Desalination by solar energy becomes one of the promising solutions to the water shortage. The demand for water and solar energy intensity are closely linked, as water needs increase during the summer when solar energy is more abundant. Solar photovoltaic thermal (PVT) systems offer a sustainable, eco-friendly method for desalination, generating both electricity and heat. The PVT system is constructed by covering a thermal collector with a PV layer. This design improves the electrical efficiency of the PV panel.[8] Utilizing PVT for desalination is an emerging application, allowing both electricity generation and heat recovery at various temperature levels. The thermal energy generated from PVT is utilized for low-grade thermal

[a]*Euromed University of Fes, UEMF, Morocco. E-mail: aliseid99@gmail.com; a.seidali@ueuromed.org*
[b]*Faculty of Chemical and Food Engineering, Bahir Dar Institute of Technology, Bahir Dar University, Bahir Dar, Ethiopia*

desalination, while the electrical energy can be used to power membrane-based desalination or be converted into thermal energy for thermal desalination.[9]

Among various desalination techniques, forward osmosis (FO) and membrane distillation (MD) are gaining popularity. In FO, water molecules pass through a porous membrane due to the osmotic pressure difference across the membrane. In MD, a hydrophobic porous membrane is used to allow vapor to pass through while retaining non-volatile matters on the feed side, driven by the vapor pressure difference across the membrane. Coupling forward osmosis with membrane distillation has shown promise as a viable alternative, especially when utilizing readily available waste heat.[10] This innovative system has several advantages: it can treat diverse water sources (seawater, brackish water, or wastewater), operates at low pressure, efficiently removes organics, salts, and pollutants, handles high salinity, and can be integrated with renewable energy sources, making it environmentally friendly.[11] By using waste heat, it lowers operational costs and carbon emissions.[11] The hybrid system also provides a double barrier against contaminants. Combining the FO and MD systems enhances their individual performance to produce high-quality water with a minimum risk of fouling.[12] FO is energy-efficient, operating under low hydraulic pressure, significantly reducing membrane fouling, and MD operates at low temperatures (40–80 °C), making it effective even with high salinity streams,[9] while also disinfecting water. Its integration with solar energy is highly recommended for water-stressed areas rich in solar radiation.[4] The system's ability to utilize waste heat and handle saline solutions enhances its potential for cost-effective desalination.[13]

Thermal energy from PVT can drive both forward osmosis and membrane distillation, while also boosting PV panel electrical output. Anand *et al.*[14] proposed integrating PVT system with FO and MD technologies. They explained how PVT's thermal energy could preheat the FO solution or aid in draw solution recovery, while its electrical energy could power auxiliary equipment.[10] The integration of PVT with FO and MD has been evaluated through laboratory-scale experiments, modeling, and simulations. Kamel *et al.*[11] reviewed the application of the FO–MD system in water treatment, highlighting the importance of water transfer balance between the two units.[7] Tashtoush *et al.*[15] noted that previous studies focused primarily on experimental investigations and testing various draw solutions, identifying a gap in integrating FO–MD with PVT systems.[11] They analyzed a PVT-driven FO–MD system incorporating phase change materials for energy storage to produce water during the night. Their system, with a capacity of 213.25 L per day, proved effective for brackish water desalination.[11] A more recent study examined the dynamic performance of PVT driven FO–MD desalination for water and electricity production.[13] Using PVT-FO–MD to produce water and energy simultaneously, reduces reliance on fossil fuels, which are major contributors of carbon emissions. Additionally, it minimizes waste heat emissions. The extended lifetime of PVT systems offsets carbon emissions more effectively compared to conventional energy sources.

After evaluating the feasibility of PVT-driven FO–MD desalination on a laboratory scale, conducting pilot-scale analyses is crucial for industrialization and assessing large-scale feasibility. However, no pilot-scale studies of the PVT-driven FO–MD system have been reported in the open literature. Bounahmidi[16] patented a method for waste heat recovery from concentrated solar power (CSP) for forward osmosis desalination applications. Building on this, a pilot FO–MD plant driven by CSP was designed.[17] CSP is a technology that collect solar energy using a thermal collector to produce high-temperature heat. Its operation is involves heating a working fluid with solar energy, which is then converted into electrical energy through a power block.[18] The waste heat from the power block is aimed to drive FO–MD desalination system. While CSP generates high-temperature thermal energy, its conversion to electrical energy requires expensive power blocks. Moreover, CSP plants utilize only the direct component of solar radiation, whereas PV systems can harness both direct and diffuse radiation. A comparison between PV and CSP shows that PV systems achieve a 13% improvement in electrical energy output while requiring 23% less area. When using a similar area, an energy improvement of 23–33% was recorded.[19] Replacing CSP with PVT systems reduces costs associated with thermal energy conversion. Our previous study numerically evaluated a PVT-driven FO–MD desalination system, claiming it as the first attempt to integrate mass and heat analyses for the entire system using Pyomo AML, validated by experimental data.[13] This study contributes to the field by designing of a PVT-driven FO–MD pilot system for the first time, along with conducting a cost and profitability analysis.

The objective of this study is to design a pilot plant integrating photovoltaic thermal (PVT), forward osmosis (FO), and membrane distillation (MD) for the simultaneous production of electricity and potable water. This pilot plant can either replace the CSP plant or operate in parallel with the CSP system previously designed by our research team. As a case study, the design is evaluated based on the annual weather conditions of Fez, Morocco. Additionally, the study conducts an economic evaluation of the pilot PVT-FO–MD plant to provide background for feasibility analysis.

2. Design of PVT-FO–MD system

2.1 PVT system design

A solar photovoltaic thermal collector combines a PV panel and a thermal collector to generate electricity and thermal energy simultaneously. PV cells are connected in series to form a module for electricity generation, while a thermal absorber attached to the back captures heat. Optimal heat transfer between the PV module and the absorber is assumed, and fluid flow tubes are integrated into the absorber through extrusion. Saline water or working fluid flows longitudinally along the PV module. Insulation is applied to the back to prevent heat loss. Multiple PVT modules are connected to meet the required power output.

Photovoltaic panels are assembled by connecting individual PV cells. Crystalline silicon cells, commonly measuring 15.6 cm

by 15.6 cm, are often used.[20] Each module typically holds either 60, 72, or 96 cells.[21–23] The module area (A_{module}) is the product of the number of cells (n) by area of a cell (A_{cell}) divide by the packing factor (PF):[24]

$$A_{module} = n \times A_{cell}/PF \quad (1)$$

The module area should be larger than cell area because cells cannot be arranged without space. For rectangular cells a 90% packing factor is reasonably considered. The input power for a certain area is estimated as:[25]

$$P_{in} = G \times A_{module} \quad (2)$$

Under standard conditions, the electrical power output of a single crystalline PV cell can be estimated using the relation:

$$P_{out} = V_{oc} \times I_{sc} \quad (3)$$

where V_{oc} is the open circuit voltage and I_{sc} is the short circuit current of a cell.

The electrical efficiency, which represents the ratio of the cell's output electrical power to its input power, can be calculated as:

$$\eta = P_{out}/P_{in} \times 100\% \quad (4)$$

The thermal output from the panel is estimated using the relation:[26]

$$P_{ther} = \dot{m} \times c_p \times (T_{out} - T_{in}) \quad (5)$$

where $\dot{m}$ is the mass flow rate of the cooling fluid, c_p is the specific heat capacity, and T_{out} and T_{in} are the outlet and inlet temperatures of the fluid, respectively. The type of PVT collector is based on a previously studied extruded absorber.[27] Such PVT collector has the advantage of higher heat transfer between the panel and absorber. The dimension of the PVT collector is 1 m by 2 m. The tube's internal diameter is 10 mm. The number of tubes per panel is decided based on the water mass flowrate considering an optimum velocity for heat to transfer from the absorber to the fluid. Based on the above description, the following table shows the values for each parameter (Table 1).

Based on the requirements, the design specifications are outlined. The required thermal power for FO and MD is supplied by the PVT panel. Therefore, the thermal output should match the conductive heat transfer from the absorber layer of the PVT collector. *i.e.* $P_{therm} = h_c \times A_{abs} \times (T_{abs} - T_f)$ where h_c is the conductive heat transfer coefficient from the absorber to the fluid, A_{abs} is the heat transfer area, and T_{abs} is the temperature of the absorber. The temperature profile of the PVT collector is estimated by applying the conservation of energy to each layer. The steady state energy balance equations on each layer are given as follows: eqn (6) for the PV layer, eqn (7) for the absorber, eqn (8) for the flowing fluid, and eqn (9) for the insulator. In these equations, G, A, η, h, T, and β represent irradiance per unit area, area of a layer, efficiency, heat transfer coefficient, temperature, and temperature coefficient, respectively.

Energy balance on the PV layer:

$$GA(1 - \eta_{PV}) = h_r A(T_{pv} - T_{sky}) + h_v A(T_{pv} - T_{amb}) + h_c A \times (T_{pv} - T_{abs}) \quad (6)$$

Energy balance on the absorber:

$$h_{cond} A(T_{pv} - T_{abs}) = h_c A_{abs,f}(T_{abs} - T_{fluid}) + h_c A(T_{abs} - T_{ins}) \quad (7)$$

Energy balance on the fluid:

$$A_s \times h_{conv}(T_{abs} - T_f) = \dot{m} \times c_p \times (T_{out} - T_{in}) \quad (8)$$

Table 1 Design parameters of the studied PVT panel

Type	Value	Comments
Open circuit voltage (V) of cell	0.6	28
Short circuit current (A) of cell	7.7	28
Electrical cell efficiency (%)	18	Estimated from I_{sc}, V_{oc}, and input irradiance at standard testing condition
Number of cells per panel	72	Standard PV panels consist 60, 72 or 96 cells. 72 cells are commonly used when bigger panels are required[29,30]
Cells dimension (cm × cm)	15.6 × 15.6	Standard crystalline solar cells dimension is considered for design purpose[30]
Standard testing condition	25 °C, 1000 W m^{-2}, 1 m s^{-1}	The standard testing condition is used for estimation of cell performance while actual condition is used for design purpose[29]
Packing factor	0.9	29
Panel area (m × m)	1 × 2	
Mass flowrate per panel (kg s^{-1})	0.004	An optimal mass flow rate for better heat transfer from absorber to fluid from previous study is used[27]
Heat capacity of the fluid (J kg^{-1} k^{-1})	4180	BW at a temperature 25 °C is assumed for the inlet fluid

Energy balance on the insulator:

$$h_{cond}A(T_{abs} - T_{ins}) = h_{conv}A(T_{ins} - T_{amb}) \quad (9)$$

The electrical power is estimated using the equation:[31]

$$P_{ele} = \eta_{ele} \times G \times A = \eta_{ele,ref} \times (1 - \beta \times (T_c - T_{ref})) \times G \times A \quad (10)$$

where η_{ref} is the reference efficiency of the PV module.

The specifications discussed above are for a single PVT collector. To design the pilot PVT collector, sizing begins with standard PV modules. The size of the pilot PVT collector is determined to operate either independently or as a substitute for the existing concentrated solar power (CSP) system when it is not operational. The CSP pilot plant was initially designed to drive the FO–MD unit. The pilot PVT unit is designed to meet the desalination unit's thermal energy requirement of 17 kW at 60 °C. This capacity was chosen to enable operation of the new design with the previously designed and currently under construction FO–MD unit. Achieving the design target involves balancing the outlet temperature (energy quality) with the generated thermal power (energy quantity), which can be controlled by adjusting the cooling fluid flow rate and improving the heat transfer design of the PVT collector. The number of PVT collectors required to produce 17 kW is estimated by dividing the pilot plant's power requirement by a single module PVT collector output. The battery storage system stabilizes power supply by compensating for fluctuations in solar energy, and storing energy to run the system when thermal power is insufficient. Modules should be arranged to fit the battery's voltage demand.

To design the heat exchanger and pumps, we need to estimate the thermal output from the absorber, which is designed to operate at the required temperature for desalination. The thermal output depends on inlet temperature (T_{in}), heat capacity of the cooling fluid (C_p), and mass flow rate ($\dot{m}$). The inlet temperature (T_{in}) is considered the ambient temperature. The mass flow rate is determined by the fluid's velocity, density, and flow area. An appropriate flow rate is considered for efficient heat transfer from the PV panel to the thermal collector. As discussed in the previous paragraph, the brackish water flow rate should maintain the balance between temperature and heat load. After estimating the thermal output and flow rate, the heat exchanger size can be determined, and pumps can be selected based on outlet temperature, head, and power requirements. The pump's power is calculated using the equation: $P = \dot{m} \times g \times h/\eta_p$ where m, h, g, and η are the flow rate, head, gravitational force, and pump efficiency, respectively.

The surface area of the heat exchanger is estimated from the following relation:

$$\dot{m}C_p(T_f - T_{out}) = \eta_{hx} \times U \times A \times LMTD \quad (11)$$

The heat transfer coefficient (U) is calculated using the relation:[32]

$$\frac{1}{U} = \frac{1}{h_i} + \frac{d_i}{2k_i}\log\left(\frac{d_o}{d_i}\right) + \frac{d_i}{d_o} \times \frac{1}{h_o} \quad (12)$$

where h_i and h_o are the heat transfer coefficients of tube and the shell fluid, k_i is the thermal conductivity, d_i and d_o are the inner and outer diameters of the tube.

2.2 FO–MD system design

The desalination unit consists of FO and MD units. The FO unit extracts water from the feed (heated saline water), while the MD unit regenerates the draw solution. The FO module contains two channels separated by porous membrane. Brackish water (BW) flows through one channel, and the draw solution flows through the other channel. The concentration difference between the two channels drives the process. FO membranes allow water to pass from the feed solution to the draw solution *via* osmotic pressure. MD recovers the draw solution's concentration after water extraction. Membrane distillation is an effective method for recovering concentrated draw solutions due to its several advantages. The process relies on a porous membrane that separates the hot feed solution from the cold permeate. The temperature difference between the two solutions creates a partial pressure gradient, which drives water vapor through the membrane's hydrophobic pores, allowing only water to pass. This temperature difference is the key factor determining the rate of vapor transport across the membrane.

The desalination system is powered by the thermal energy from the PVT collector. The desalination units (MD and FO) are sized to operate based on the average available energy from the PVT. A constant BW flow rate and draw solution concentration are considered. The FO unit's design depends on the thermal energy collected, BW flow rate, and module size.

Using mass conservation principles, the water flux (J_w), the module area (A_{FO}), and water density (ρ) determine the output brine flow rate ($\dot{m}_{out}$). The total mass balance defines the inlet flow rate ($\dot{m}_{in}$) as the sum of the outlet brine flow rate ($\dot{m}_{out}$) and the water and salt fluxes across the membrane.

$$\dot{m}_{in,fd} = \dot{m}_{out,fd} + J_w \times A_{FO} \times \rho - J_s A_{FO} \quad (13)$$

To calculate the solute material balance on the feed side of the forward osmosis (FO) unit, where C represents the salt concentration in the inlet and outlet streams, we use the following equation where Q and C represent volumetric flow rate and salt concentration, respectively:

$$Q_{in,fd}C_{in,fd} + J_s A_{FO} = Q_{out,fd}C_{out,fd} \quad (14)$$

The water flux through the FO membrane is determined by the equation:[33] J_w = permeablity $\times$ ($\Pi_{draw} - \Pi_{feed}$) where Π signifies the osmotic pressure of the draw or feed solution. We also performed similar overall and component material balances on the draw solution stream.

$$\dot{m}_{out,d} = \dot{m}_{in,d} + J_w \times A_{FO} \times \rho - J_s A_{FO} \text{ and } Q_{in,d}C_{in,d} = Q_{out,d}\text{-}C_{out,d} + J_s A_{FO} \quad (15)$$

We assume a saline water concentration of 10 000 ppm and a NaCl draw solution with a concentration of 1 M. By solving the

combined set of material balance equations, we can determine the required membrane dimensions. The water flux of the FO unit is temperature-dependent. Energy balance equations for both the feed and draw sides of the FO module are included in the calculations. The energy balance equations are as follows:

$$\dot{m}_{fd} \times c_p \times T_{fd} = J_w \times A_{FO} \times \rho \times T_{FO} + m_b \times c_b \times T_b \text{ and } J_w \times A_{FO} \times \rho \times T_{FO} + \dot{m}_d \times c_d \times T_{MD} = \dot{m}_c \times c_c \times T_c \quad (16)$$

where the subscripts fd, b, c, and d indicate the fluid inlet to FO, brine from FO, circulation fluid (diluted draw solution), and concentrated draw solution, respectively. It should be noted that the heat exchanger tube side outlet is the inlet to the feed side of the FO unit.

The size of the membrane distillation unit depends on the input flow rate from the FO system. The sizing between the FO and the MD unit should be compatible to maintain a continuous flow throughout the system without any overflow or depletion. Similar to the FO unit, material balances are conducted on the MD unit to determine its required size.

The mass flux (J_v) through the porous membrane in the MD unit can be described by Darcy's law:[13]

$$J_v = C_m(\Delta P_v) = C_m(P^0_{vf}\gamma_{vf} - P^0_{vp}) \quad (17)$$

where C_m is the mass transfer coefficient, P_v represents the partial vapor pressure, and γ_v denotes the activity coefficient of the brackish water or draw solution. The Antoine equation is used to determine the vapor pressure (P^0_v) on the feed and permeate sides (P_{vf} and P_{vp}) as follows:

$$P_{vf} = \exp\left(23.1964 - \frac{3816.44}{T_{vf} - 46.13}\right) \text{ and } P_{vp} = \exp\left(23.1964 - \frac{3816.44}{T_{vp} - 46.13}\right) \quad (18)$$

As indicated by the Antoine equation, the partial pressure is temperature-dependent. This underscores the importance of mass and energy transfer analysis, which primarily occurs in the MD unit. Heat transfer involves convective heat transfer in the feed channel, conduction across the membrane, and heat of vaporization. The heat transfer equation across the membrane is given as: $Q_{total} = Q_{cond} + Q_{vap}$ where Q_{cond} is conduction heat flux through the membrane and Q_{vap} is vaporization heat flux. The conduction and convection heat fluxes are expressed as:

$$Q_{cond} = k_m/\delta_m \times (T_{mf} - T_{mp}) \text{ and } Q_{vap} = J_w \times \Delta H_v \quad (19)$$

Here, ΔH_v is the latent heat of vaporization of water given by $\Delta H_v = 1000(-2.426 \times T_{mf} + 2503)$.[34]

The design incorporates several parameters. For brevity, the parameters used in previous works are not repeated here; readers are referred to previously published articles.[13,27] However, changes in the mass transfer coefficient (C_m) of the MD unit are as follows:[35,36]

$$C_m = \frac{M_w}{RT\delta_m}\left(\frac{1}{\frac{1}{R_v} + \frac{1}{R_{kn} + R_M}}\right) \quad (20)$$

where the resistances R_v, R_{kn}, and R_m are given as:[35] $R_v = \varepsilon r^2 P/8\tau\mu_g$, $R_m = \varepsilon PD/\tau P_{air}$, and $R_{kn} = 2r\varepsilon/3\tau\sqrt{8RT/M_w}$.

The thickness (δ_m) of the MD membrane is taken as 150 μm. The membrane porosity (ε) is 0.7, and complexity of the membrane pathways or tortuosity (τ), calculated as $\tau = (2-\varepsilon)^2/\varepsilon$, is 2.41. The membrane radius (r) is 0.22 μm. The dynamic viscosity (μ_g) of the gas is given as a function of temperature.

$$\mu_g = -3.036 \times 10^{-11} \times T^2 + 6.638 \times 10^{-8} \times T + 1.356 \times 10^{-6} \quad (21)$$

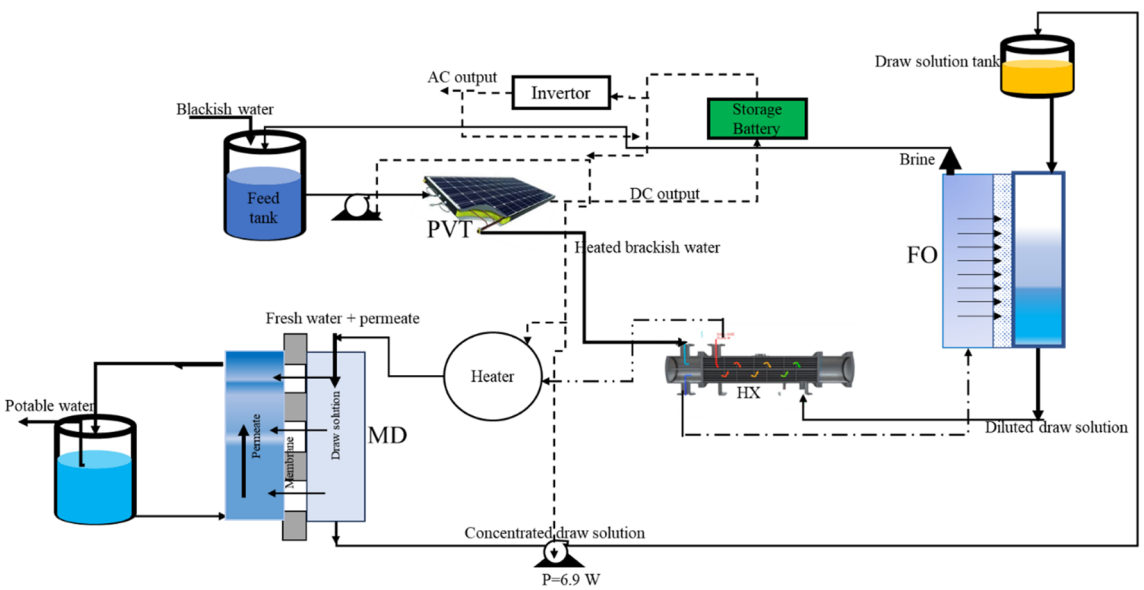

Fig. 1 PVT driven FO–MD desalination pilot unit.

The designed PVT-FO–MD system is illustrated in Fig. 1. Solar energy heats the PVT collector, generating electricity and thermal energy. The electricity powers auxiliary equipment, is stored for later use during sunless periods, or is converted to AC for household applications. Simultaneously, BW circulates through the PVT collector, absorbing thermal energy and heating up to 60 °C. This heated BW then transfers its heat to the diluted draw solution stream before entering the FO unit. Membrane in the FO unit, separate the BW into concentrated BW and fresh water. The concentrated brackish water mixes with inlet BW. Fresh water permeates from the feed side of the FO unit and mixes with the draw solution on the draw side resulting in a dilute draw solution. The latter enters a heat exchanger for further heating using the PVT thermal energy. Subsequently, the MD unit separates the heated mixture into fresh water and draw solution. The recovered draw solution cycles back to the FO unit, while the produced fresh water flows directly to consumers. Pumps are used to ensure the circulation of draw solution and to provide continuous feed.

2.3 Simulation of PVT-FO–MD system

The system of equations developed in Sections 2.1 and 2.2 were solved simultaneously using the algorithm shown in Fig. 2. This algorithm was further employed to analyze the yearly performance of the pilot plant. It requires creating a Pyomo model in the Python environment. The required inputs for this algorithm include BW flow rate, irradiance, wind velocity, ambient temperature, dimensions, and feed solution and draw solute concentrations. The outputs, including temperatures in the PVT layer, outlet temperature of the fluid from the PVT, FO, and MD units, water fluxes, as well as thermal and electrical powers, were estimated. The system of equations developed in Section 2.1 and 2.2 are implemented as functions with appropriate naming conventions. Boundary and initial conditions are also specified. The equations were solved after initialization, and convergence was tested. If convergence is achieved, the simulation stops; otherwise, the initialization is adjusted. The results were then analyzed. This algorithm has been applied in our previous studies. Readers interested in further details are referred to our previously published articles.[13,27] For this algorithm, the inputs required are brackish water flow rate, rate of radiation per unit area, the concentration of BW, and the concentration of draw solution.

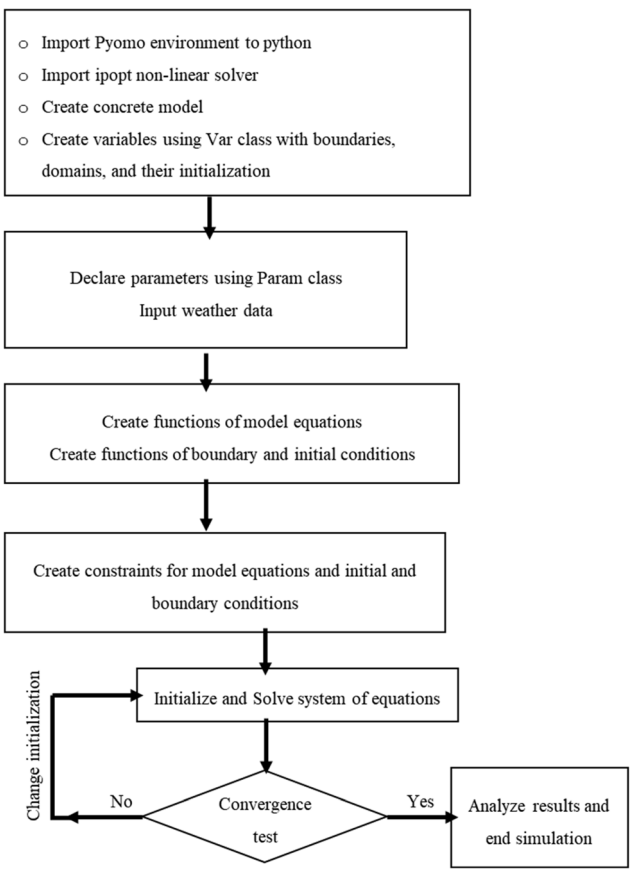

Fig. 2 Simulation algorithm.

3. Results and discussion

The capacity of the pilot PVT unit is determined based on the thermal energy demand of the desalination unit as discussed in the methodology. For design purposes, a yearly average irradiance of 710 W m^{-2}, an ambient temperature of 24.8 °C, and wind velocity of 1.6 m s^{-1} are used. The battery stores excess energy generated by the PVT system when irradiance levels are high. This stored energy can be used to supplement the desalination unit's energy demand during periods of low irradiance. Under these conditions, the PVT should generate the required thermal energy for desalination. When estimation results in a decimal, the number of panels is rounded up. The daily operational period is limited to 10 hours, considering the hours of available solar irradiance. Local metrological data was considered to understand its effect on the performance of the pilot plant.

Table 2 provides a summary of the specifications for the pilot plant. Output variables such as FO and MD water flux, intermediate and outlet temperatures, electrical and thermal powers, heat exchanger area and load, pump power, and MD area were estimated by varying input parameters, including panel area and number, BW flowrate, inlet temperature, and FO area.

Based on the discussion in the design section of the pilot PVT-FO–MD unit, the plant flowsheet, with appropriate labeling of stream flowrates, temperatures, and concentrations, is given in Fig. 11. For ease of steady state analysis, the feed BW should mix with the brine at ambient conditions. A saline water flow rate of 0.196 kg s^{-1} is required to provide the necessary thermal power. The PVT collector was estimated at 98 m^2, generating 9.39 kW of electrical power. The average daily electrical energy was 93.9 kW h. The saline water temperature at the heat exchanger outlet was 38 °C, serving as the inlet to the FO unit. The FO unit size is 3.3 m^2, with a water flux of 8.14 LMH. The diluted draw solution, heated to 43.5 °C in the heat exchanger, was further heated to 60 °C using an electrical heater. The MD

Table 2 Pilot plant design specifications results

Parameter	Amount	Comments
Single panel area (m^2)	2	PV cells performance was estimated at standard conditions
Number of panels	49	Panel performance was estimated at 710 W m^{-2} irradiance, 24.8 °C ambient temperature, and 1.6 m s^{-1} wind velocity
FO unit membrane area (m^2)	3.3	Feed side active layer membrane is considered FO area increased to 3.8 m^2 to analyze its effect
MD unit membrane area (m^2)	9.36	The size of MD is decided to maintain continuous flow (constant flow rate circulation of draw solution) throughout the loop MD area increased to 11.6 m^2 to maintain the flow when FO area increased to analyze its effect
Number of pumps	2	Two pumps with a maximum of 10 m head and 75% pump efficiency are considered One pump is used to feed saline water to the PVT unit and another pump is used for circulation of draw solution between FO and MD
PVT inlet saline water flow rate (L h^{-1})	705.6	The flow rate is optimized to provide a balance between the outlet temperature and amount of thermal energy demanded
FO water flux (LMH)	8.14	Selective layer on the feed side mode is considered
MD water flux (LMH)	2.87	Air gap membrane distillation unit is considered
MD permeate flow rate (L h^{-1})	712	This flow rate is estimated based on simultaneous calculation of all the mass and energy balance equations. This flow rate was estimated to maintain the required water flux
Saline water inlet temperature (°C)	25 °C	
Saline water outlet temperature (°C)	48 °C	The outlet temperature from the PVT collector
Electrical power produced (kW)	9.39	
Thermal power produced (kW)	17.21	Designed with a 20% increment above the desalination unit demand
Heat load of the heat exchanger (kW)	8.17	The heat exchanged in the exchanger is transferred to the diluted draw solution. The fluid enters at 48 °C and leaves at 38 °C A 0.3 kW thermal energy is considered as a loss in the heat exchanger
Area of the heat exchanger (m^2)	6.8	

unit area was estimated at 9.36 m^2, with a water flux of 2.87 LMH. The concentrated draw solution, at a flow rate of 0.237 kg s^{-1} and a temperature of 33 °C, is recirculated to the FO unit.

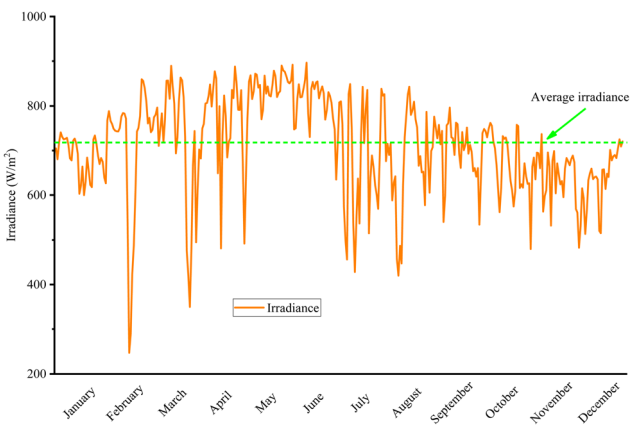

Fig. 3 Average irradiance.[37]

To analyze the yearly performance of the PVT-FO–MD system, we utilized weather data from Fez, Morocco. Irradiance data for 2019 was extracted from the National Renewable Energy Laboratory database.[37] The mean irradiance was found to be 710 W m^{-2}, with significant daily fluctuations. Fig. 3 depicts the average irradiance data from 8:00 to 18:00 h.

3.1 Annual energy and water production

The average electrical power production is shown in Fig. 4. Electrical power production between March and June is generally above demand, while from July to October, it is near the average. During the rest of the year, production tends to fall below average. The minimum recorded electrical power was 3.28 kW in February, while the maximum was 11.26 kW in June, with an average of 9.28 kW. Based on the design specifications, the system can produce 33 872 kW h electrical energy annually. These fluctuations are attributed to variations in daylight length and irradiance intensity throughout the year.

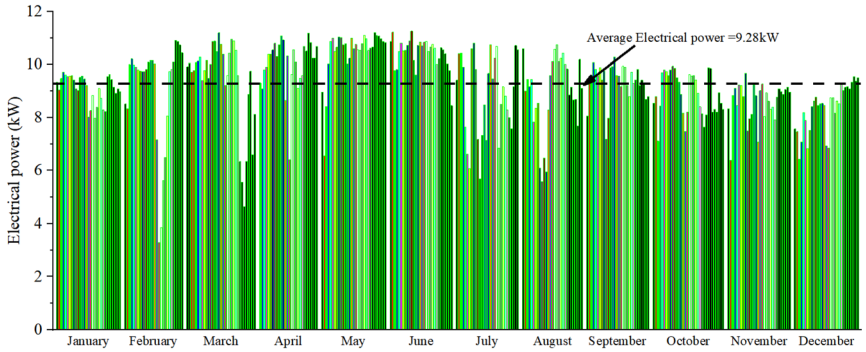

Fig. 4 Electrical power production.

The thermal power is estimated using the relation: $\eta_{ther} = \dot{m}_f \times c_p \times (T_{out} - T_{in})/(G \times A)$. Higher thermal power was generated in March to June, following a similar trend to the electrical power. The lowest thermal power was recorded in November, December, and January, with a minimum of 16.61 kW, while the maximum was 21.86 kW. The average thermal power was 18.04 kW. The annual thermal energy production was estimated to be 65 846 kW h. The yearly thermal power production is displayed in Fig. 5.

The water fluxes were also analyzed, with both MD and FO water fluxes showing variation throughout the year. The FO water flux remains relatively stable, ranging from 8.13 and 8.29 LMH, while the MD water flux fluctuates with irradiance, varying between 2.72 and 4.25 LMH. This variation is attributed to changes in fluid temperature during the analysis. Fig. 6 illustrates the FO and MD water fluxes.

The average water production is 29.27 L h^{-1}, with a minimum of 25.57 L h^{-1} and a maximum of 39.95 L h^{-1}. Fig. 7 illustrates the yearly water production. The estimated annual

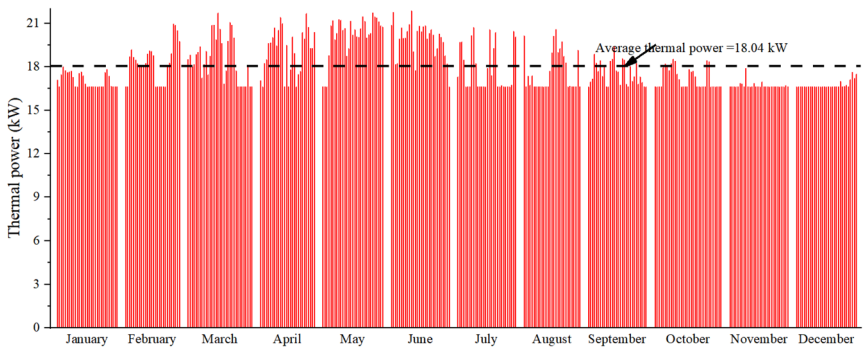

Fig. 5 Thermal power production.

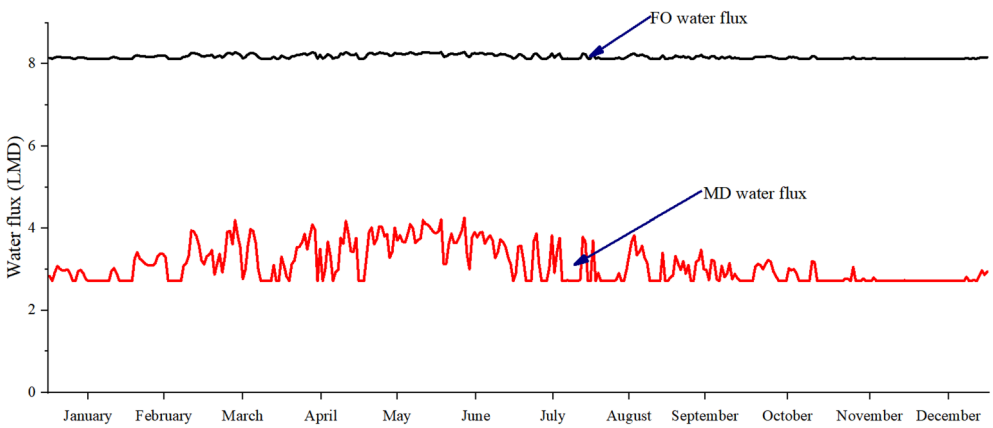

Fig. 6 FO and MD water fluxes.

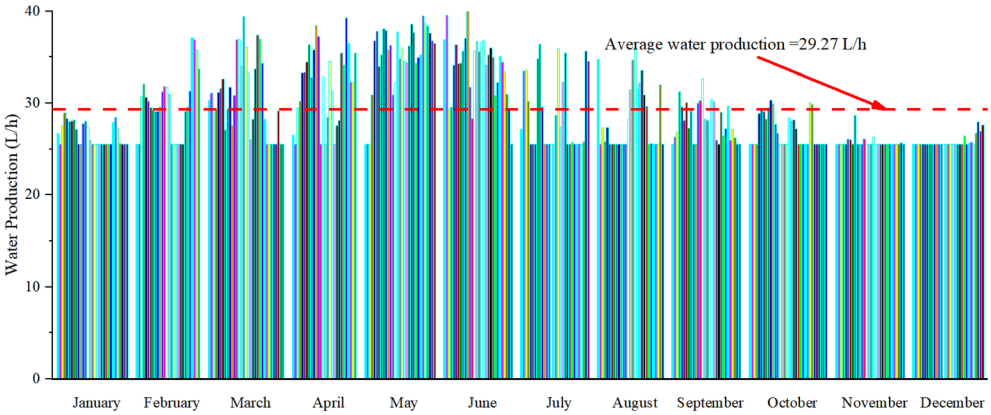

Fig. 7 Average water production based on the initial membrane area.

water production volume is 106.84 m^3. Similar to electricity and thermal power, higher water production was observed in May and June. Increased energy and water production during the summer is crucial due to higher demand. In winter, water demand is lower, but energy demand increases for heating. In summer, both water and cooling energy demands are high. Previous studies indicate that MD requires between 1 kW h m^{-3} and 499 kW h m^{-3} of energy for water desalination.[14] The current study, which integrates both FO and MD systems, demonstrates specific energy consumption levels that are comparable to these findings.

While water flux depends on factors such as osmotic pressure, temperature, permeability, and others, increasing the membrane area can enhance the water production rate. Increasing the FO area to 3.8 m^2 and the corresponding MD area to 11.6 m^2 results in an average water production of 34.65 L h^{-1}, as shown in Fig. 8. However, this change requires additional heating due to the increased mass of the draw solution. The temperature in the heat exchanger is lowered, particularly at lower irradiance, which in turn reduces the water flux and the water production. Despite this, the system can produce 346.5 L per day if operated for 10 hours at the average production rate.

The flow rate and irradiance primarily influence the performance of the PVT collector, while temperature and concentration play significant roles in the desalination unit. Several combinations of input flowrate, irradiance, and feed concentrations were tested as part of the sensitivity analysis. Irradiance values of 500, 700, and 1000 W m^{-2}; feed flowrates of 529.2, 720 and 882 L h^{-1}; and BW concentrations of 3000, 5000, and 10 000 mg L^{-1} were evaluated. The effect of these parameters on the system's performance are illustrated in Table 3. Each input significantly impacts system performance, with different inputs affecting different outputs. For instance, an increase in feed concentration generally reduces water flux and production, especially at lower irradiance levels. This occurs because a higher feed concentration decreases the concentration gradient, which is the driving force. Similarly, thermal power increases with both irradiance and flowrate as irradiance improves temperature and increased flowrate enhances latent heat transfer. The highest thermal power (29.34 kW) was achieved at the highest BW flowrate and lowest BW concentration regardless of irradiance. The highest electrical power (12.26 kW) was recorded at the highest BW flow rate and irradiance. The maximum FO water flux (9.84 LMH) was observed at the lowest cooling fluid flowrate, highest irradiance, and lowest BW concentration. Similarly, the maximum MD water flux (6.5 LMH) occurred at the lowest BW flowrate and highest irradiance, irrespective of feed concentration. Maximum water

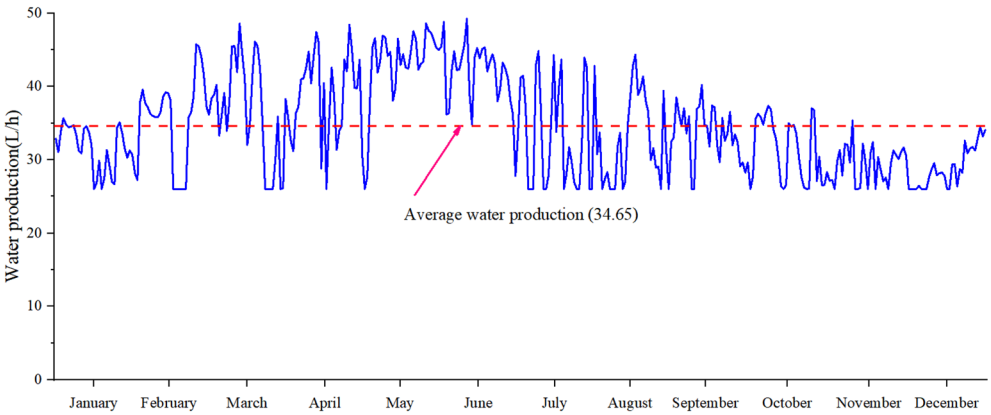

Fig. 8 Average water production based on increased membrane area.

Table 3 Effect of feed flow rate, irradiance, and concentration effects

	Flow rate (Liter h^{-1})	Irradiance (W m^{-2})	Feed concentration (mg $Liter^{-1}$)	Thermal power (kW)	Electrical power (kW)	FO flux (LMH)	MD flux (LMH)	Water production (L h^{-1})
1	529.2	500	3000	17.59	6.33	9.69	4.8	45.15
2			5000	16.1	6.46	9.23	4.12	38.74
3			10 000	12.42	6.77	8.12	2.71	25.45
4		700	3000	17.59	8.86	9.69	4.8	45.15
5			5000	16.1	9.04	9.23	4.12	38.74
6			10 000	14.44	9.24	8.2	3.44	32.32
7		1000	3000	20.76	12.12	**9.84**	**6.5**	**61.11**
8			5000	20.72	12.12	9.45	**6.5**	**61.11**
9			10 000	20.76	12.12	8.46	**6.5**	**61.11**
10	720	500	3000	23.47	6.17	9.69	4.81	45.22
11			5000	21.5	6.31	9.24	4.13	38.84
12			10 000	16.61	6.65	8.13	2.72	25.6
13		700	3000	23.47	8.63	9.69	4.81	45.22
14			5000	21.5	8.83	9.24	4.13	38.84
15			10 000	16.95	9.28	8.14	2.81	26.39
16		1000	3000	24.4	12.2	9.73	5.15	48.44
17			5000	24.4	12.2	9.34	5.15	48.44
18			10 000	24.4	12.2	8.37	5.15	48.44
19	882	500	3000	**29.34**	6	9.69	4.81	45.23
20			5000	26.88	6.16	9.24	4.13	38.85
21			10 000	20.77	6.53	8.13	2.72	25.59
22		700	3000	**29.34**	8.4	9.69	4.81	45.23
23			5000	26.88	8.62	9.24	4.13	38.85
24			10 000	20.77	9.15	8.13	2.72	25.59
25		1000	3000	**29.34**	12	9.69	4.81	45.23
26			5000	27.26	**12.26**	9.25	4.23	39.8
27			10 000	27.26	**12.26**	8.29	4.23	39.8

production (61.11 L h^{-1}) was achieved under similar conditions to those for maximum MD water flux.

3.2 Economic analysis of the pilot PVT-FO–MD unit

Process designs are typically conducted to provide information for cost estimation. Estimating the required investment and production costs is needed for profitability assessments. Such design estimations aid in deciding between alternative and optimized designs. A cost analysis was performed to assess the feasibility of the PVT-driven FO–MD pilot plant. Cost and profitability analysis concepts are provided in plant design and economics books, such as those by Peters and Timmerhaus.[38] Therefore, the cost analysis in this study is based on this book unless specialized studies are available for specific cases. The total capital investment includes fixed capital (consisting of direct and indirect costs) and working capital.[38]

Direct capital covers expenses like PVT panels, FO and MD modules, pumps, heat exchanger, and their installation, while indirect fixed capital involves manufacturing and plant facilities. Capital cost estimation is based on equipment purchasing costs. Those costs were collected from similar studies or manufacturers' and suppliers' databases, and average market prices were considered for cost estimation. When data from these sources is for equipment with a different capacity, the exponential rule is applied to scale up or down, accounting for cost index.[38,39] Working capital is the capital necessary for the plant's operation. Operation and maintenance costs are estimated as 3% of total capital cost, based on standards.[40] Table 4 details the estimated costs for the proposed PVT-FO–MD system, based on the equipment sizes calculated in Section 3.

The capital cost is high, but governments often support renewable energy plants through subsidies, tax incentives, or loan programs due to their environmental benefits. Such intervention can further reduce costs and improve the feasibility of these projects. The energy used for water production is considered intermediate and is not included in the profitability analysis. A portion of the electricity produced is used for makeup heating in MD desalination, which is not considered part of the saleable output. The system produces 292.7 L of water and 22.7 kW h of electrical output daily. Based on current market prices, the estimated selling price for water can be as high as \$5.95 per cubic meter (as in Norway),[47] and global electricity prices range from \$0.002 to 0.458 per kW h.[48] Various water and electricity prices were evaluated to determine the minimum selling price for project feasibility. Cashflow and net present value (NPV) were estimated based on these prices, projecting an annual income of approximately 25 178 USD. Cashflow refers to the difference between income and expenses, while NPV represents the sum of all cashflows. The rate of return on investment is estimated at 11.84%, calculated as the ratio of yearly profit to initial investment multiplied by 100. At a minimum selling price of \$3 per kW h, cumulative cashflow and NPV, as illustrated in Fig. 9, show the project breaking even

Table 4 Estimated cost of the system

No.	Item	Cost (USD)	Remark	Ref.
1	Pilot scale PVT collector	27 790.00	The cost is estimated by scaling the data given for a 1.36 m^2 single panel (450 USD) from a ref. 41 cited a manufacturer	42
2	FO unit	31 500.00	8.14 L m^{-2} h^{-1} water flux is considered	43
3	MD unit	39 000.00	2.87 L m^{-2} h^{-1} water flux is considered 26.86 L h^{-1} potable water produced	
4	Balance of system (wiring, charger control, invertor, and battery)	11 750.00	15% loss is considered	44
5	Heat exchanger	14 000.00	Sheel and tube heat exchanger is considered Heat transferred to the cold side is 8.47 kW (0.3 kW heat is lost in the heat exchanger)	45
6	Pumps	2000.00	Enough height (10 m) is considered to compensate pressure drop in the pipe	
7	Storage tanks	1000.00		46
8	Membrane	500.00	To be changed every 2 years	
9	Electrical heater	7000.00		
10	Total purchasing cost	134 540.00		
11	Installation, piping and instrumentations	20 181.00	15% of the purchasing cost	
12	Indirect costs	38 680.25	Supervision, contractor, and contingency	
13	Fixed capital cost	193 401.25	Direct cost + indirect cost	
14	Total capital cost	212 741.38	Sum of working and fixed capital cost 10% of fixed capital cost is considered for working capital	

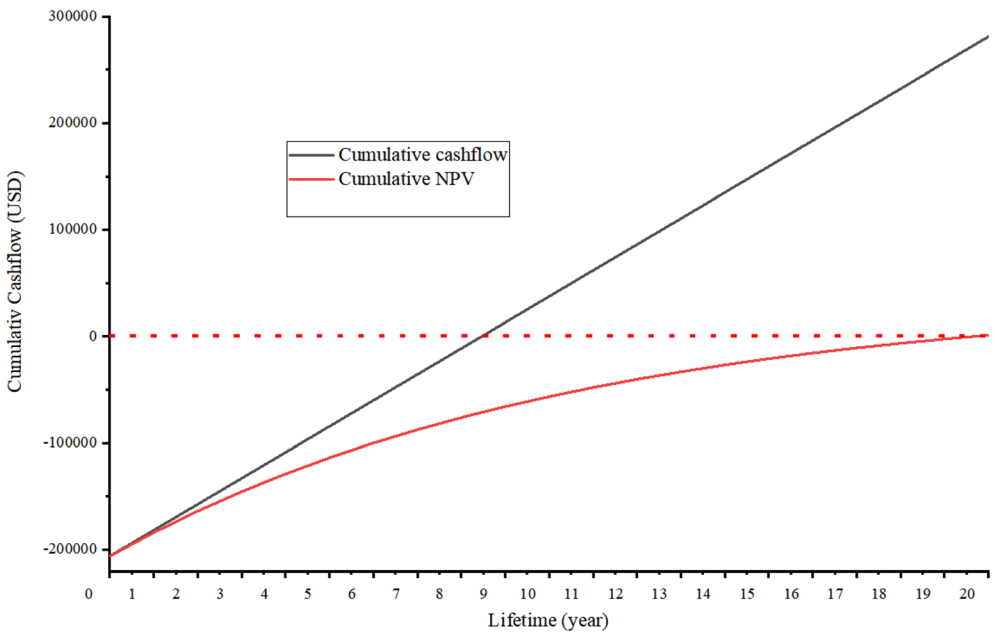

Fig. 9 Cumulative cashflow and net present value.

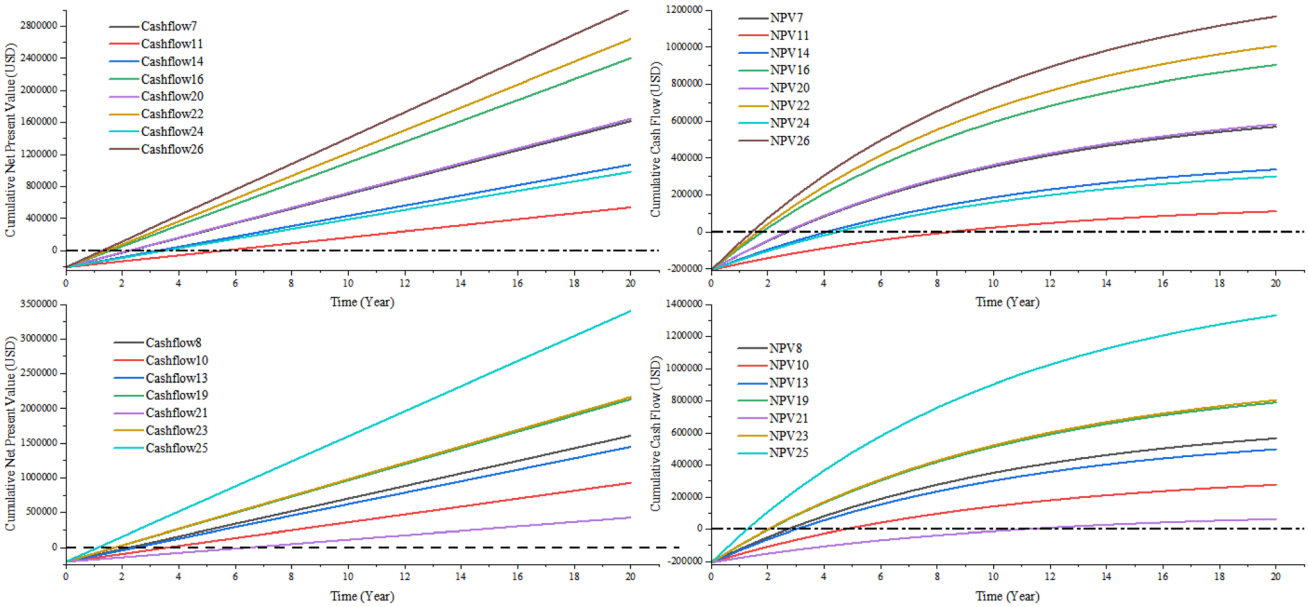

Fig. 10 Profitability analysis at different flowrates, irradiances, and feed concentration (based on data on Table 3).

in year 9. With a 10% interest rate, the project's NPV turns positive after 19 years.

We have analyzed the effect of different flow rate, irradiance, and feed concentration combinations on cashflow and NPV. These combinations are derived from the data in Table 3. Among the 27 input combinations, options 1, 2, 3, 4, 5, 6, 12, and 15 were found to be infeasible. Options number 9, 17, 18, and 27 are a duplicate of other combinations. The cumulative cashflow and cumulative net present values for the remaining combinations are plotted in Fig. 10. The left-side subfigures show the cumulative net present value, while the right-side subfigures display the cumulative cashflow. Among these combinations, option 25 (at highest irradiance, highest feed flowrate, and lowest feed concentration) yields the highest cumulative cashflow and NPV. Conversely, option 21 (at the lowest irradiance, highest feed flowrate, and highest feed concentration) results in the lowest cumulative cashflow and NPV.

The advantages of the PVT driven FO–MD system are demonstrated through the pilot scale profitability analysis. The results indicate that this system is competitive with conventional systems. Its ability to operate in off-grid areas makes it feasible for both small-scale and large-scale applications. Additionally, its low-grade thermal energy utilization ensures effectiveness under various weather conditions. The system's capability to treat a wide range of feedwater sources further enhances its versatility and supports diverse applications. In summary, it has significant potential for industrial application following a detailed economic evaluation.

4. Conclusion

A pilot scale design of a PVT-driven FO–MD desalination was developed to evaluate process feasibility, water and electricity production costs, and potential scalability for industrial uses. The system could reduce the capital cost associated with energy conversion if concentrated solar power is implemented. While PVT collectors are more expensive than standard PV panels, they offer improved electrical efficiency and additional thermal power generation, making them more efficient overall. Using average yearly weather data, the system produces 9.28 kW of electrical power, 18.04 kW of thermal power, and 29.27 L h^{-1} of water. Increasing the desalination unit sizes boosts average water production to 34.65 L h^{-1}. The capital cost required to run the project is 212 741.38 USD. The system generates 292.7 L of water and 22.7 kW h of electricity per day. The return on investment is 11.84%, with a breakeven point at 9 years. The NPV becomes positive after 19 years at a 10% interest rate. Although this kind of system has not yet been commercialized, its environmental benefits are clear. However, further studies are recommended to enhance its market competitiveness.

Abbreviation

Symbol, meaning

PVT	Photovoltaics thermal
FO	Forward osmosis
MD	Membrane distillation
CSP	Concentrated solar power
NPV	Net present value
A	Area (m^2)
PF	Packing factor
V	Voltage (V)
I	Current (A)
P	Power (W)/pressure (Pa)
G	Irradiance (W m^{-2})
C_p	Specific heat capacity (J kg^{-1} K^{-1})
T	Temperature (°C)
h	Heat transfer coefficient (W m^{-2} K^{-1})

C_m	Mass transfer coefficient (s m^{-3})
LMTD	Log mean temperature difference
U	Over all heat transfer coefficient (W m^{-2} K^{-1})
D	Diameter (m)
K	Thermal conductivity (W m^{-1} K^{-1})
J	Water flux (m^3 m^{-2} s^{-1})
C	Concentration (kg m^{-3})
Q	Volumetric flow rate (m^3 s^{-1})/heat flux (W m^{-2})
H	Latent heat (J)
M	Molecular mass (kg)
R	Resistance (m s^{-1})
r	Radius (m)
$\dot{m}$	Mass flow rate (kg s^{-1})
ρ	Density (kg m^{-3})
Π	Osmotic pressure (Pa)
η	Efficiency (%)
ε	Porosity (m)
δ	Thickness (m)
τ	Membrane pathways or tortuosity (m)
μ	Viscosity (N s m^{-2})

Data availability

Data used for this study is provided in the manuscript.

Conflicts of interest

There are no conflicts to declare.

Appendix

Acknowledgements

The authors gratefully acknowledge the scholarship support provided by Euromed University of Fes through the African Scientific Research and Innovation (ASRIC) program.

References

1 R. A. Alenazi, I. H. Alsohaimi, M. R. El-Aassar, Y. A. El-Ossaily, E. K. Alenezy, S. J. F. Alanazi, *et al.*, Comparative analysis of high-performance UF membranes with sulfonated polyaniline: Improving hydrophilicity and antifouling capabilities for water purification, *Sep. Purif. Technol.*, 2025, **353**, 128409, DOI: 10.1016/j.seppur.2024.128409.

2 M. N. AlMallahi, J. Mustafa, A. H. Al-Marzouqi and M. Elgendi, Research progress and state-of-the-art on solar membrane desalination, *Case Stud. Chem. Environ. Eng.*, 2024, **10**, 100825, DOI: 10.1016/j.cscee.2024.100825.

3 M. U. Hameed, Z. Amjad, A. B. Al, A. El Jery, H. M. A. Hassan, L. Ali, *et al.*, Recent progress in 2D-MXene-based membranes for water treatments; fabrication, properties, and advanced desalination application, *Desalination*, 2025, **599**, 118462, DOI: 10.1016/j.desal.2024.118462.

4 X. Han, F. Ding, J. Huang and X. Zhao, Hybrid nanofluid filtered concentrating photovoltaic/thermal-direct contact membrane distillation system for co-production of electricity and freshwater, *Energy*, 2023, **263**, 125974, DOI: 10.1016/j.energy.2022.125974.

5 Y. Zheng, R. A. Caceres Gonzalez, K. B. Hatzell and M. C. Hatzell, Large-scale solar-thermal desalination, *Joule*, 2021, **5**, 1971–1986, DOI: 10.1016/j.joule.2021.07.005.

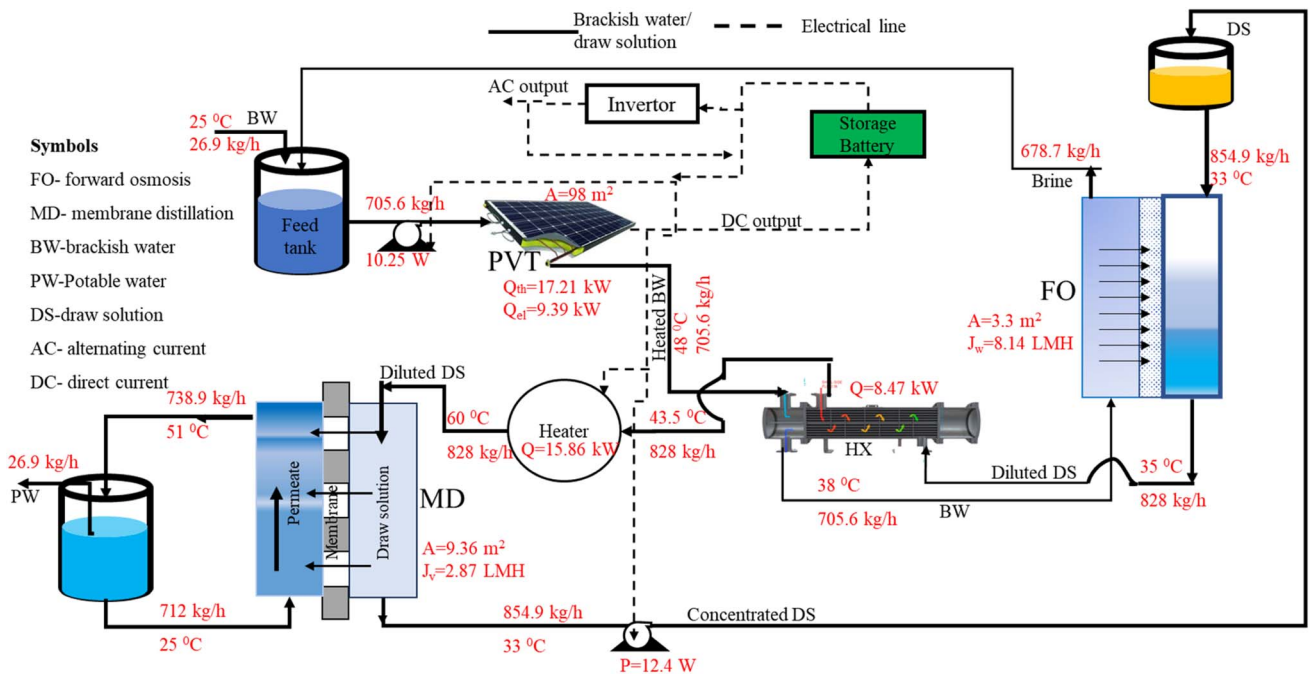

Fig. 11 Pilot PVT-FO–MD unit flow diagram with specifications.

6 S. M. Alawad, R. B. Mansour, F. A. Al-Sulaiman and S. Rehman, Renewable energy systems for water desalination applications: a comprehensive review, *Energy Convers. Manage.*, 2023, **286**, 117035, DOI: **10.1016/j.enconman.2023.117035**.

7 E. Ogunniyi and B. S. Richards, Renewable energy powered membrane technology: power control management for enhanced photovoltaic-membrane system performance across multiple solar days, *Appl. Energy*, 2024, **371**, 123624, DOI: **10.1016/j.apenergy.2024.123624**.

8 K. Bilen and İ. Erdoğan, Effects of cooling on performance of photovoltaic/thermal (PV/T) solar panels: a comprehensive review, *Sol. Energy*, 2023, **262**, 111829, DOI: **10.1016/j.solener.2023.111829**.

9 W. He, G. Huang and C. N. Markides, Synergies and potential of hybrid solar photovoltaic-thermal desalination technologies, *Desalination*, 2023, **552**, 116424, DOI: **10.1016/j.desal.2023.116424**.

10 S. Reddy, K. Dey, D. Dsilva Winfred Rufuss, S. Arulvel and T. Akinaga, Forward osmosis desalination: a critical review focussing on recent advancements in draw solution recovery techniques for enhanced efficiency and regeneration, *J. Environ. Chem. Eng.*, 2024, **12**, 113968, DOI: **10.1016/j.jece.2024.113968**.

11 A. H. Kamel, R. A. Al-Juboori, M. al-shaeli, B. Ladewig, S. S. Ibrahim and Q. F. Alsalhy, Potential application of hybrid forward osmosis – membrane distillation (FO-MD) system for various water treatment processes, *Process Saf. Environ. Prot.*, 2023, **180**, 1023–1052, DOI: **10.1016/j.psep.2023.10.053**.

12 S. M. Shalaby, M. E. Zayed, F. A. Hammad, A. S. Menesy and A. R. A. Elbar, Recent advances in membrane distillation hybrids for energy-efficient process configurations: technology categorization, operational parameters identification, and energy recovery strategies, *Process Saf. Environ. Prot.*, 2024, **190**, 817–838, DOI: **10.1016/j.psep.2024.07.098**.

13 A. S. Ali and T. Bounahmidi, Coupling of photovoltaic thermal with hybrid forward osmosis-membrane distillation: energy and water production dynamic analysis, *J. Water Process Eng.*, 2024, **64**, 105710, DOI: **10.1016/j.jwpe.2024.105710**.

14 B. Anand, R. Shankar, S. Murugavelh, W. Rivera, K. Midhun Prasad and R. Nagarajan, A review on solar photovoltaic thermal integrated desalination technologies, *Renew. Sustainable Energy Rev.*, 2021, **141**, 110787, DOI: **10.1016/j.rser.2021.110787**.

15 B. Tashtoush, G. M. Al and N. Tashtoush, Advancing solar-powered hybrid FO-MD desalination: integrating PVT collectors and PCM for sustainable water production in residential building, *Energy Build.*, 2024, **313**, 114246, DOI: **10.1016/j.enbuild.2024.114246**.

16 T. Bounahmidi, *Solar thermal power plant cooling system by coupling to a direct osmosis brackish water desalination process*, MA 34695B1, 2013.

17 I. Chaoui, S. Abderafi, S. Vaudreuil and T. Bounahmidi, Development of a forward osmosis desalination process coupled with a CSP plant and analysis of the phenomena involved, PhD thesis, Mohammed V University of Rabat Mohammadia School of Engineers, 2022.

18 R. Klaimi, S. Y. Alnouri and M. Stijepović, Design and thermo-economic evaluation of an integrated concentrated solar power – Desalination tri-generation system, *Energy Convers. Manage.*, 2021, **249**, 114865, DOI: **10.1016/j.enconman.2021.114865**.

19 U. Desideri, F. Zepparelli, V. Morettini and E. Garroni, Comparative analysis of concentrating solar power and photovoltaic technologies: technical and environmental evaluations, *Appl. Energy*, 2013, **102**, 765–784, DOI: **10.1016/j.apenergy.2012.08.033**.

20 X. Ye, S. Zou, K. Chen, J. Li, J. Huang, F. Cao, *et al.*, Efficient multi-crystalline silicon solar cells with novel nanoscale pseudo-pyramid texture, *Adv. Funct. Mater.*, 2014, **24**, 6708–6716, DOI: **10.1002/adfm.201401589**.

21 A. Woyte, J. Nijs and R. Belmans, Partial shadowing of photovoltaic arrays with different system configurations: literature review and field test results, *Sol. Energy*, 2003, **74**, 217–233, DOI: **10.1016/S0038-092X(03)00155-5**.

22 A. Chub, D. Vinnikov, O. Korkh, M. Malinowski and S. Kouro, Ultrawide voltage gain range microconverter for integration of silicon and thin-film photovoltaic modules in DC microgrids, *IEEE Trans Power Electron.*, 2021, **36**, 13763–13778, DOI: **10.1109/TPEL.2021.3084918**.

23 D. Vinnikov, A. Chub, E. Liivik, R. Kosenko and O. Korkh, Solar optiverter – a novel hybrid approach to the photovoltaic module level power electronics, *IEEE Trans. Ind. Electron.*, 2019, **66**, 3869–3880, DOI: **10.1109/TIE.2018.2850036**.

24 J. Ji, J. Han, T. Chow, H. Yi, J. Lu, W. He, *et al.*, Effect of fluid flow and packing factor on energy performance of a wall-mounted hybrid photovoltaic/water-heating collector system, *Energy Build.*, 2006, **38**, 1380–1387, DOI: **10.1016/j.enbuild.2006.02.010**.

25 M. Wang, J. Peng, Y. Luo, Z. Shen and H. Yang, Comparison of different simplistic prediction models for forecasting PV power output: assessment with experimental measurements, *Energy*, 2021, **224**, 120162, DOI: **10.1016/j.energy.2021.120162**.

26 E. Arslan, M. Aktaş and Ö. F. Can, Experimental and numerical investigation of a novel photovoltaic thermal (PV/T) collector with the energy and exergy analysis, *J. Clean. Prod.*, 2020, **276**, 123255, DOI: **10.1016/j.jclepro.2020.123255**.

27 A. S. Ali and T. Bounahmidi, Dynamic performance analysis of a photovoltaic thermal (PVT) collector with an extruded absorber using python optimization modeling object (pyomo), *Appl. Therm. Eng.*, 2024, **247**, 123028, DOI: **10.1016/j.applthermaleng.2024.123028**.

28 L. Peng, Y. Sun and Z. Meng, An improved model and parameters extraction for photovoltaic cells using only three state points at standard test condition, *J. Power Sources*, 2014, **248**, 621–631, DOI: **10.1016/j.jpowsour.2013.07.058**.

29 P. Dupeyrat, C. Ménézo, M. Rommel and H. M. Henning, Efficient single glazed flat plate photovoltaic-thermal hybrid collector for domestic hot water system, *Sol. Energy*, 2011, **85**, 1457–1468, DOI: **10.1016/j.solener.2011.04.002**.

30 A. J. Beinert, P. Romer, M. Heinrich, M. Mittag, J. Aktaa and D. H. Neuhaus, The effect of cell and module dimensions on thermomechanical stress in PV modules, *IEEE J. Photovoltaics*, 2020, **10**, 70–77, DOI: **10.1109/JPHOTOV.2019.2949875**.

31 M. Al-Hrari, İ. Ceylan, K. Nakoa and A. Ergün, Concentrated photovoltaic and thermal system application for fresh water production, *Appl. Therm. Eng.*, 2020, **171**, 115054, DOI: **10.1016/j.applthermaleng.2020.115054**.

32 S. Saha and N. Hasan, Numerical evaluation of thermohydraulic parameters for diverse configurations of shell-and-tube heat exchanger, *Results Eng.*, 2024, **23**, 102509, DOI: **10.1016/j.rineng.2024.102509**.

33 R. Colciaghi, R. Simonetti, L. Molinaroli, M. Binotti and G. Manzolini, Potentialities of thermal responsive polymer in forward osmosis (FO) process for water desalination, *Desalination*, 2022, **519**, 115311, DOI: **10.1016/j.desal.2021.115311**.

34 A. M. Karam, A. S. Alsaadi, N. Ghaffour and T. M. Laleg-Kirati, Analysis of direct contact membrane distillation based on a lumped-parameter dynamic predictive model, *Desalination*, 2017, **402**, 50–61, DOI: **10.1016/j.desal.2016.09.002**.

35 S. Adnan, M. Hoang, H. Wang and Z. Xie, Commercial PTFE membranes for membrane distillation application: effect of microstructure and support material, *Desalination*, 2012, **284**, 297–308.

36 S. O. Olatunji and L. M. Camacho, Heat and mass transport in modeling membrane distillation configurations: a review, *Front. Energy Res.*, 2018, **6**, 130, DOI: **10.3389/fenrg.2018.00130**.

37 *NSRDB: National Solar Radiation Database*, 2023, **https://nsrdb.nrel.gov/data-viewer**, accessed 23 September, 2023.

38 M. S. Peters and K. D. Timmerhaus, *Plant Design and Economics for Chemical Engineers*, 4th edn., McGraw-Hill Chemical Engineering Series, 1991.

39 G. Towler and R. Sinnott, in *Chemical engineering design principles, practice and economics of plant and process design*, Elsevier Inc., 2008.

40 M. Mortadi, A. El Fadar and O. Achkari Begdouri, 4E analysis of photovoltaic thermal collector-based tri-generation system with adsorption cooling: annual simulation under moroccan climate conditions, *Renewable Energy*, 2024, **221**, 119828, DOI: **10.1016/j.renene.2023.119828**.

41 M. A. Obalanlege, J. Xu, C. N. Markides and Y. Mahmoudi, Techno-economic analysis of a hybrid photovoltaic-thermal solar-assisted heat pump system for domestic hot water and power generation, *Renewable Energy*, 2022, **196**, 720–736, DOI: **10.1016/j.renene.2022.07.044**.

42 *How much solar panels cost?*, n.d., **https://us.sunpower.com/solar-resources/how-much-do-solar-panels-cost**, accessed 1 September, 2024.

43 S. J. Im, S. Jeong and A. Jang, Forward osmosis (FO)-reverse osmosis (RO) hybrid process incorporated with hollow fiber FO, *NPJ Clean Water*, 2021, **4**, 51, DOI: **10.1038/s41545-021-00143-0**.

44 V. Bertsch, J. Geldermann and T. Lühn, What drives the profitability of household PV investments, self-consumption and self-sufficiency?, *Appl. Energy*, 2017, **204**, 1–15, DOI: **10.1016/j.apenergy.2017.06.055**.

45 *Corrosion Resistance Heat Exchanger*, n.d., **https://www.alibaba.com/product-detail/Corrosion-Resistant-Heat-Exchanger-Industrial-stainless_1600228068113.html?spm=a2700.details.0.0.660559ddCMCPAJ**, accessed 7 August, 2024.

46 *How Much Does a Water Tank Cost?*, n.d., **https://www.angi.com/articles/how-much-does-water-tank-replacement-cost.htm**, accessed 1 September, 2024.

47 *Water Prices Compared in 36 EU-Cities*, 2024, **https://www.waternewseurope.com/water-prices-compared-in-36-eu-cities/**, accessed 21 October, 2024.

48 *Cost of Electricity by country*, 2024, **https://worldpopulationreview.com/country-rankings/cost-of-electricity-by-country**, accessed 21 October, 2024.